Effect of surface waves on the secondary Bjerknes force experienced by bubbles in a microfluidic channel

Alexander A. Doinikov, Thomas Combriat, Pierre Thibault, and Philippe Marmottant
LIPhy, UMR 5588, CNRS/Université Grenoble-Alpes, Grenoble, F-38401, France
(Received 28 June 2016; published 10 August 2016)

An analytical expression is derived for the secondary Bjerknes force experienced by two cylindrical bubbles in a microfluidic channel with planar elastic walls. The derived expression takes into account that the bubbles generate two types of scattered acoustic waves: bulk waves that propagate in the fluid gap with the speed of sound and Lamb-type surface waves that propagate at the fluid-wall interfaces with a much lower speed than that of the bulk waves. It is shown that the surface waves cause the bubbles to form a bound pair in which the equilibrium interbubble distance is determined by the wavelength of the surface waves, which is much smaller than the acoustic wavelength. Comparison of theoretical and experimental results demonstrates good agreement.

DOI: 10.1103/PhysRevE.94.023105

I. INTRODUCTION

The dynamics of ultrasound-driven bubbles in a microfluidic channel is characterized by specific conditions. First, bubbles are squeezed between two closely spaced channel walls, which makes their form close to cylindrical. Second, bubble oscillations set in motion not only the fluid inside the channel, but the elastic channel walls as well. As a result, two types of scattered acoustic waves arise in the fluid gap, namely, bulk waves that propagate with the speed of sound, and Lamb-type surface waves whose propagation speed is much smaller than the sound speed in the fluid [1–3]. These conditions are observed experimentally to change radically acoustic radiation forces acting between bubbles [1].

The interaction between two bubbles in an acoustic field is conventionally described in terms of secondary Bjerknes force [4,5]. The classical theory of this phenomenon for two spherical bubbles was developed by C. A. Bjerknes and his son V. F. K. Bjerknes [6]. Their theory predicts that, if the driving frequency is higher or lower than the resonance frequencies of both bubbles, the bubbles attract each other; if the driving frequency is between the resonance frequencies of the bubbles, the bubbles repel each other. It should be emphasized that the Bjerknes theory implies that the direction of the force remains the same at all times. However, later studies, both theoretical and experimental, have shown that the force can change sign when the interbubble distance is changed [7–14]. In particular, attraction can change to repulsion at small distances comparable to bubble radii [12], and the direction of the force can change repeatedly when the interbubble distance is comparable to or more than the acoustic wavelength [13]. This means that two bubbles can form a stable bound pair with a fixed separation distance.

However, until recently there was no information on acoustic radiation forces experienced by cylindrical bubbles in microfluidic systems. Rabaud *et al.* [1] reported on such investigations. Their experimental observations show that acoustically excited microfluidic bubbles can form a bound structure in which equilibrium interbubble distances are much smaller than the acoustic wavelength but still remain large compared to bubble radii. It was also found that the equilibrium distance was independent of the acoustic pressure amplitude and bubble size. These results cannot be explained by existing theories for secondary Bjerknes forces. Rabaud *et al.* [1] have assumed that, in addition to bulk waves, bubbles emit surface acoustic waves that propagate at the channel walls and whose wavelength is much smaller than that of the bulk waves. Based on this assumption, they developed a semiqualitative model that was able to explain their observations.

The present study is inspired by the results of Rabaud *et al.* [1]. Our purpose is to derive rigorously an analytical formula for the secondary Bjerknes force experienced by two cylindrical bubbles in a microfluidic channel and to check this formula against experimental data. The derivation is based on the results of our recent work [3], where analytical solutions were obtained for both bulk and Lamb-type surface waves produced by a cylindrical bubble in a fluid channel with planar elastic walls.

II. THEORY

The geometry of the problem under consideration is shown in Fig. 1. Two gas cylindrical bubbles are confined in a fluid channel with planar elastic walls. The bubbles undergo radial oscillations in response to an imposed acoustic pressure field. The bubble oscillations induce bulk scattered waves in the surrounding fluid and elastic surface waves in the channel walls. The surface waves, in turn, produce acoustic perturbations in the fluid. As a result, there are two types of scattered acoustic waves in the fluid: the bulk waves whose speed, c_f, is the speed of sound in the fluid, and Lamb-type surface wave that propagate at the fluid-wall interfaces and whose speed, c_s, is equal to the speed of the surface waves in the channel walls. This process is described in [3], where it is shown that c_s is much smaller than c_f. Our purpose is to calculate the secondary Bjerknes force between the bubbles with allowance made for both types of scattered acoustic waves. To describe the fluid motion, we introduce two systems of cylindrical coordinates originated at the bubble centers as shown in Fig. 1(b).

Let us calculate the force on bubble 1. It is given by [5]

$$\boldsymbol{F}_1 = -\left\langle \int p_2 \boldsymbol{n}_1 ds \right\rangle, \tag{1}$$

where p_2 is the fluid pressure produced by bubble 2 at the position of bubble 1, $\boldsymbol{n}_1$ is the outward unit normal to the

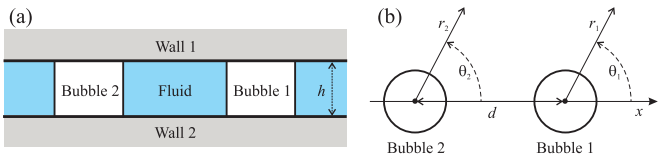

FIG. 1. Two cylindrical bubbles in a microfluidic channel. (a) Side view. (b) Top view.

surface of bubble 1, $\langle\cdot\rangle$ means time averaging, and the integral is taken over the surface of bubble 1. Changing the integration over the bubble surface to that over the bubble volume and keeping up to leading terms, one has

$$\boldsymbol{F}_1 = -\left\langle \int \nabla p_2 dV \right\rangle = -\langle V_1 \nabla p_2 \rangle, \tag{2}$$

where V_1 is the time-varying volume of bubble 1 and ∇p_2 is taken at the center of bubble 1. Let us assume that the time-varying radius of bubble 1 is given by

$$R_1(t) = R_{10}[1 + a_1 \exp(-i\omega t)], \tag{3}$$

where R_{10} is the equilibrium radius, a_1 is the dimensionless pulsation amplitude, and ω is the angular driving frequency. It should be emphasized that Eq. (3) means that the bubble pulsation is treated as linear. In microfluidic experiments, the bubble pulsation amplitude is on the order of a few percent of the equilibrium bubble radius. For example, Fig. 4 of Ref. [15] shows that the pulsation amplitude of two interacting bubbles with radii 35 μm is 0.8 μm, i.e., 2.3% of the equilibrium radius. Therefore, the linear approximation of the bubble pulsation is justified.

Substituting Eq. (3) into Eq. (2) and averaging over the acoustic period, one obtains

$$\boldsymbol{F}_1 = -\pi h R_{10}^2 \mathrm{Re}\{a_1^* \nabla p_2\}, \tag{4}$$

where h is the height of the microfluidic channel, Re means "the real part of," and the asterisk indicates the complex conjugate.

To calculate p_2, we use the results of our recent work [3]. It follows from Eqs. (2.62), (2.73), (2.76), and (2.87) of Ref. [3] that p_2 can be represented by

$$p_2(r_2) = -\frac{\rho_f \omega^2 a_2}{k_f H_1^{(1)}(k_f R_{20})}\left[R_{20} - \frac{k_t q_2}{\pi\mu} I_{fr}(R_{20},0)\right] \times H_0^{(1)}(k_f r_2) - \frac{\rho_f \omega^2 q_2 a_2}{\pi\mu} I_p(r_2,0), \tag{5}$$

where the following designations are used:

$$q_2 = -2\pi\gamma\left(P_0 + \frac{\sigma_f}{R_{20}}\right) R_{20}^2 \varepsilon_2. \tag{6}$$

ρ_f is the fluid density, a_2 is the dimensionless pulsation amplitude of bubble 2, $k_f = \omega/c_f$ is the wave number of the bulk wave, $H_n^{(1)}$ is the Hankel function of the first kind of order n, R_{20} is the equilibrium radius of bubble 2, $k_t = \omega/c_t$ is the wave number of the transverse wave in the channel walls, c_t is the speed of the transverse wave [16], μ is the shear modulus of the wall material, the functions I_{fr} and I_p are given by Eqs. (2.65) and (2.67) in Ref. [3], γ is the ratio of specific heats of the gas in the bubbles, P_0 is the hydrostatic pressure in the fluid, σ_f is the surface tension coefficient for the fluid-gas interfaces, and ε_2 is a fitting parameter that is introduced in Ref. [3] to describe the action of the bubble on the channel walls. The values of this parameter for different frequencies are given in Ref. [3]. According to Ref. [3], the first term on the right-hand side of Eq. (5) is due to the bulk wave and the second term is due to the surface waves.

Substitution of Eq. (5) into Eq. (4) yields

$$\boldsymbol{F}_1 = -\pi h \rho_f \omega^2 R_{10}^2 R_{20} \boldsymbol{e}_{21} \mathrm{Re}\{G_2(d) a_1^* a_2\}, \tag{7}$$

where $\boldsymbol{e}_{21}$ is the unit vector directed from bubble 2 to bubble 1, d is the distance between the bubble centers, and the dimensionless function G_2 is defined by

$$G_2(r_2) = \left[1 - \frac{k_t q_2}{\pi\mu R_{20}} I_{fr}(R_{20},0)\right] \frac{H_1^{(1)}(k_f r_2)}{H_1^{(1)}(k_f R_{20})} - \frac{q_2}{\pi\mu R_{20}} \frac{dI_p(r_2,0)}{dr_2}. \tag{8}$$

Note also that it follows from Eqs. (2.65) and (2.67) in Ref. [3] that $dI_p(r_2,0)/dr_2 = -k_t I_{fr}(r_2,0)$. In order to get the force on bubble 2, it is sufficient to write the above equations interchanging indices 1 and 2 that denote the bubbles.

It remains to calculate a_1 and a_2. To this end, we use Eq. (2.88) of Ref. [3]. According to that equation, considering also that we have two bubbles, a_1 and a_2 can be represented as

$$a_1 = -\frac{P_a + p_2(d)}{D_1}, \quad a_2 = -\frac{P_a + p_1(d)}{D_2}, \tag{9}$$

where P_a is the amplitude of the imposed acoustic pressure field and D_j $(j = 1, 2)$ is given by

$$D_j = 2\gamma P_0 + \frac{(2\gamma - 1)\sigma_f}{R_{j0}} - \frac{\rho_f \omega^2 R_{j0}^2 H_0^{(1)}(\alpha_{fj})}{\alpha_{fj} H_1^{(1)}(\alpha_{fj})} + \frac{2\gamma \rho_f \alpha_{tj}^2 \varepsilon_j}{\rho_s}\left(P_0 + \frac{\sigma_f}{R_{j0}}\right) \times \left[I_p(R_{j0},0) - \frac{\alpha_{tj} H_0^{(1)}(\alpha_{fj})}{\alpha_{fj} H_1^{(1)}(\alpha_{fj})} I_{fr}(R_{j0},0)\right], \tag{10}$$

with $\alpha_{fj} = k_f R_{j0}$, $\alpha_{tj} = k_t R_{j0}$, and ρ_s being the wall density. The quantity $p_1(d)$ is the fluid pressure produced by bubble 1 at the center of bubble 2. It is calculated by Eq. (5), where index 2, denoting bubble 2, should be replaced by 1. Solving Eqs. (9) simultaneously, one obtains

$$a_1 = \frac{(B_2 - D_2)P_a}{D_1 D_2 - B_1 B_2}, \quad a_2 = \frac{(B_1 - D_1)P_a}{D_1 D_2 - B_1 B_2}, \tag{11}$$

where

$$B_j = -\frac{\rho_f \omega^2}{\pi\mu}\left\{\frac{H_0^{(1)}(k_f d)}{k_f H_1^{(1)}(k_f R_{j0})}[\pi\mu R_{j0} - k_t q_j I_{fr}(R_{j0},0)] + q_j I_p(d,0)\right\}. \tag{12}$$

It is interesting to compare Eq. (7) with the expression for the force which was derived by Rabaud *et al.* [1] on the basis of qualitative considerations. Their considerations lead to the

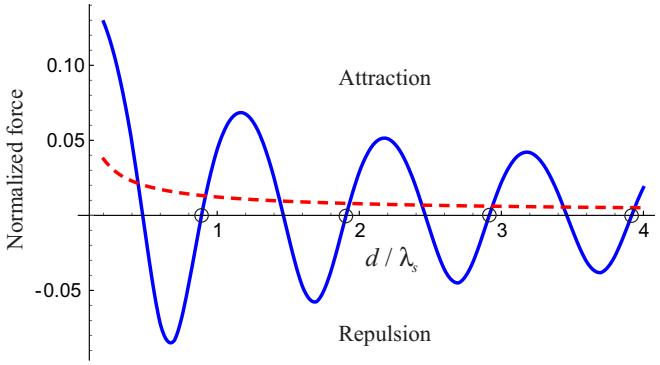

FIG. 2. Secondary Bjerknes force versus interbubble distance. Two bubbles with radii 25 μm are excited at 50 kHz. The solid line shows the force when both bulk and surface waves are taken into account. The dashed line shows the force when the surface waves are neglected. The open circles show equilibrium states.

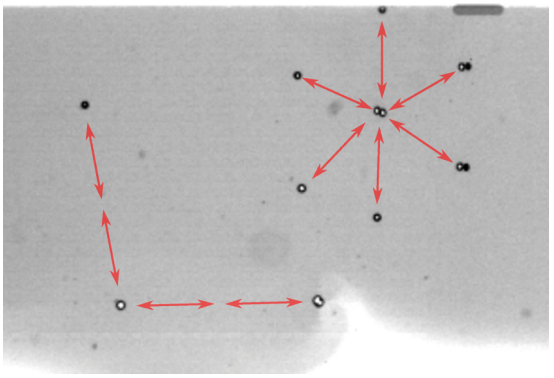

FIG. 3. Experimental snapshot of an ordered structure formed by bubbles in a PDMS channel under exposure to ultrasound: A view through the transparent top of the channel. The driving frequency is 85 kHz and the bubble radii are approximately 20–25 μm. The equilibrium distances between the bubbles in the hexagon structure are about 386 μm. The distances between the bubbles on the left side of the figure are equal to twice the equilibrium distance in the hexagon.

result that the potential of the Bjerknes force Φ_B depends on the distance between the bubbles d as follows:

$$\Phi_B(d) \sim \frac{\cos(k_s d)}{\sqrt{d}}, \tag{13}$$

where $k_s = \omega/c_s$ is the wave number of the surface waves in the channel walls. The force potential in Eq. (7) is given by the function

$$\Phi_{F_1}(d) = \pi h R_{10}^2 \mathrm{Re}\{a_1^* p_2(d)\}. \tag{14}$$

This equation, in combination with Eq. (5), shows that, if we neglect the contribution of the bulk waves compared to that of the surface waves and take into account that the function $I_p(d,0)$ behaves as the Hankel function $H_0^{(1)}(k_s d)$ at large d (see Ref. [3]), we obtain the following result:

$$\Phi_{F_1}(d) \sim I_p(d,0) \sim H_0^{(1)}(k_s d) \sim \frac{\exp(ik_s d)}{\sqrt{k_s d}}, \tag{15}$$

where the last term follows from the asymptotic expansion of the Hankel function for large arguments [17]. Equation (15) shows that the assumptions of Rabaud *et al.* [1] are in agreement with our theory.

III. NUMERICAL EXAMPLES AND COMPARISON WITH EXPERIMENTAL DATA

Numerical calculations were made assuming that the fluid in the channel is water and the gas in the bubbles is air. Correspondingly, the following physical parameters were used: $\rho_f = 998\,\mathrm{kg/m^3}$, $\sigma_f = 0.072\,\mathrm{N/m}$, $c_f = 1481\,\mathrm{m/s}$, $P_0 = 101.3\,\mathrm{kPa}$, and $\gamma = 1.4$. The channel walls were assumed to be made of a polydimethylsiloxane (PDMS) elastomer with the following parameters: $\rho_s = 970\,\mathrm{kg/m^3}$, Young's modulus $E = 1.6\,\mathrm{MPa}$, and Poisson's ratio $\sigma = 0.499$. E and σ are necessary to calculate μ, c_t, and c_s [3,16,18]. The channel height was taken to be $h = 25\,\mu$m.

Figure 2 exemplifies the dependence of the secondary Bjerknes force on the interbubble distance d. The solid line shows the force when both bulk and surface waves are taken into account. For comparison, the dashed line shows what happens if the surface waves are neglected and only the bulk waves are allowed for. The calculation was made for bubbles with radii $R_{10} = R_{20} = 25\,\mu$m, excited at a frequency $f = 50\,\mathrm{kHz}$ and acoustic pressure amplitude $P_a = 1\,\mathrm{kPa}$. The force is normalized by $P_a^2/(\rho_f \omega^2)$ and d is normalized by the wavelength of the surface waves $\lambda_s = c_s/f$. The positive and negative values of the force correspond to attraction and repulsion, respectively. Equilibrium states arise when attraction changes to repulsion with decreasing d. They are circled on the solid curve. Note that, as the dashed curve shows, if the surface waves are absent, the force is permanently attractive. It should be mentioned that, in view of the linear approximation of the bubble pulsation, the force is linearly dependent on P_a^2. Therefore, the change of the acoustic pressure amplitude changes only the magnitude of the force and does not affect the behavior of the curves in Fig. 2.

Figure 3 is an experimental snapshot that provides an idea of the bubble behavior in a microfluidic channel under exposure to ultrasound. The snapshot was made using a microfluidic setup described in Ref. [1]. It gives a view through the transparent top of a PDMS channel. As one can see on the right upper side of Fig. 3, bubbles self-organize in a hexagonlike structure with fixed interbubble distances. The depicted arrows, which are equal in length, allow one to compare the distances. It is interesting to note that on the left of the hexagon, there are bubble pairs in which the equilibrium distance is twice as large as that between the bubbles in the hexagon. This observation corroborates the prediction of Rabaud *et al.* [1], as well as that of Fig. 2, that equilibrium states can arise at multiple distances. Note also that there are two bubbles in contact in the center of the hexagonlike structure. Figure 2 shows that at separations smaller than about $\lambda_s/2$ the force is attractive. Thus, if bubbles are at such distances, they approach each other up to contact. The bubble pair in the center of the hexagon demonstrates this case.

Figure 4 checks theoretical predictions against experimental measurements. It shows the equilibrium interbubble distance as a function of the driving frequency. The

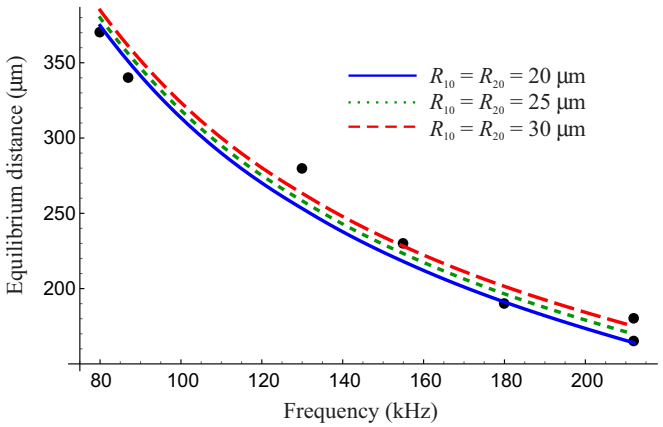

FIG. 4. Equilibrium interbubble distance versus driving frequency. The circles show experimental data adopted from Ref. [1]. The curves show theoretical results for three bubble pairs with different radii.

experimental data are depicted by circles. They were adopted from the work by Rabaud *et al.* [1] (see Fig. 3 in their article). The microfluidic setup used by Rabaud *et al.* [1] did not allow one to determine the amplitude of the driving acoustic pressure, P_a. However, the same setup was used in the work of Mekki-Berrada *et al.* [15], where measurements were made for bubble pulsation amplitudes under similar experimental conditions. For example, for bubbles with radii 35 μm, the pulsation amplitude was 0.8 μm. Theoretical estimations, based on the theory developed in Ref. [3], show that such pulsation amplitudes correspond to values of P_a about 1–2 kPa. These data confirm that the linear approximation of the bubble pulsation is valid under the experimental conditions of Ref. [1]. The experimental data of Ref. [1] were obtained for the pairs of equal bubbles with radii in the range 20–30 μm. Rabaud *et al.* [1] report that their measurements do not demonstrate a noticeable dependence on bubble size. The theoretical results are presented by three curves that were calculated for three pairs of equal bubbles with radii 20 μm (solid), 25 μm (dotted), and 30 μm (dashed). In this calculation, we have assumed that the equilibrium state observed in the experiment is a state that corresponds to the circle beside $d/\lambda_s = 2$ in Fig. 2. With this assumption, the theoretical curves are in good agreement with the experimental data. Note also that they show an insignificant dependence on bubble size, which conforms to the observations of Rabaud *et al.* [1]. For the sake of completeness, it should be mentioned that the calculations were made at $P_a = 1$ kPa. However, in view of the linearity of the bubble pulsation, the value of P_a does not affect the results of Fig. 4. The effect of the acoustic pressure amplitude becomes important in the case of nonlinear bubble pulsations. At present, however, experimental and theoretical investigations need to be made on the interaction force between microfluidic bubbles exposed to nonlinear excitation. This problem requires a separate consideration.

IV. CONCLUSION

An analytical expression has been derived for the secondary Bjerknes force experienced by two cylindrical bubbles confined in a microfluidic channel with planar elastic walls. The derived expression takes into account two types of scattered waves generated by the bubbles, namely, the bulk waves, which propagate in the fluid gap with the speed of sound and the Lamb-type surface waves, which propagate at the fluid-wall interfaces with the speed equal to that of the surface waves in the channel walls. It has been shown that the surface waves make the bubbles form a bound pair in which the equilibrium distance between the bubbles is determined by the wavelength of the surface waves. As a result, equilibrium states can arise at interbubble distances that are much smaller than the acoustic wavelength. Comparison of theoretical and experimental data has demonstrated good agreement. The obtained results are of immediate interest for investigations into microfluidics.

ACKNOWLEDGMENT

This research has received funding from the European Research Council under the European Union's Seventh Framework Programme (FP7/2007-2013)/ERC Grant Agreement No. 614655 "Bubbleboost."

[1] D. Rabaud, P. Thibault, M. Mathieu, and P. Marmottant, Phys. Rev. Lett. **106**, 134501 (2011).
[2] F. Mekki-Berrada, P. Thibault, and P. Marmottant, Phys. Fluids **28**, 032004 (2016).
[3] A. A. Doinikov, F. Mekki-Berrada, P. Thibault, and P. Marmottant, Proc. R. Soc. A **472**, 20160031 (2016).
[4] L. A. Crum, J. Acoust. Soc. Am. **57**, 1363 (1975).
[5] T. G. Leighton, *Acoustic Bubble* (Academic Press, London, 1994).
[6] V. F. K. Bjerknes, *Fields of Force* (Columbia University Press, New York, 1906).
[7] Yu. A. Kobelev, L. A. Ostrovskii, and A. M. Sutin, JETP Lett. **30**, 395 (1979).
[8] E. A. Zabolotskaya, Sov. Phys. Acoust. **30**, 365 (1984).
[9] H. N. Oguz and A. Prosperetti, J. Fluid Mech. **218**, 143 (1990).
[10] N. A. Pelekasis and J. A. Tsamopoulos, J. Fluid Mech. **254**, 501 (1993).
[11] P. L. Marston, E. H. Trinh, J. Depew, and J. Asaki, in *Bubble Dynamics and Interface Phenomena*, edited by J. R. Blake, J. M. Boulton-Stone, and N. H. Thomas (Kluwer Academic, Dordrecht, 1994), pp. 343–353.
[12] A. A. Doinikov and S. T. Zavtrak, Phys. Fluids **7**, 1923 (1995).
[13] A. A. Doinikov and S. T. Zavtrak, J. Acoust. Soc. Am. **102**, 1424 (1997).
[14] R. Mettin, I. Akhatov, U. Parlitz, C.-D. Ohl, and W. Lauterborn, Phys. Rev. E **56**, 2924 (1997).
[15] F. Mekki-Berrada, T. Combriat, P. Thibault, and P. Marmottant, J. Fluid Mech. **797**, 851 (2016).
[16] I. A. Viktorov, *Rayleigh and Lamb Waves: Physical Theory and Applications* (Plenum Press, New York, 1967).
[17] M. Abramowitz and I. N. Stegun, *Handbook of Mathematical Functions* (Dover Publications, New York, 1965).
[18] L. D. Landau and E. M. Lifshitz, *Theory of Elasticity* (Pergamon Press, Oxford, 1970).